Appl. Phys. A (2016) 122:291
DOI 10.1007/s00339-016-9817-0

Applied Physics A
Materials Science & Processing

CrossMark

The role of ammonization on chemical bonding and optical properties of nickel-catalyzed gallium nitride nanowire

Umesh Rizal[1] · Bhabani S. Swain[2] · Bibhu P. Swain[1]

Received: 11 January 2016 / Accepted: 16 February 2016 / Published online: 7 March 2016
© Springer-Verlag Berlin Heidelberg 2016

Abstract Nickel-catalyzed gallium nitride nanowires (GaN-NWs) were grown on p-type Si (100) substrates using Ga_2O_3 powder and NH_3, N_2, and H_2 as precursor gases in chemical vapor deposition reactor. The GaN-NWs were characterized by atomic force microscopy (AFM), Fourier transform infrared spectroscopy, Raman spectroscopy, and photoluminescence (PL) spectroscopy to investigate microstructural, structural, optical, and chemical bonding networks of GaN-NW films. AFM shows the formation of GaN-NWs with different diameter. The room temperature PL spectra of GaN-NWs show a broad blue emission band centered at 2.54, 2.69, 2.81, 2.89, and 2.94 eV, which are associated with different electronic transitions. The stokes shift of GaN-NWs reveals the existence of prominent transverse optic and longitudinal optic (LO) peak at 548 and 795 cm^{-1}, respectively. However, the pronounced blue shifting of LO peak was observed with increasing NH_3 flow rate indicates considerable stress in NWs.

1 Introduction

Gallium nitride nanowire (GaN-NW) is a wideband gap (3.4 eV) semiconductor material, used efficiently in optoelectronic, sensors, and high-temperature devices [1–3]. To date, several techniques have been used to synthesize GaN-NWs such as thermal evaporation [4], radio frequency magnetron sputtering [5], atmospheric pressure CVD [6], low-pressure CVD [7], metallo-organic CVD [2], and hot wire CVD [8]. Sundaram et al. [9] have synthesized GaN epitaxial layers on silicon substrate with different NH_3 flow rates and observed that the concentration of Ga like vacancies increases with increasing NH_3 flow rate. Nam et al. [6] reported the morphological evolution of GaN nanostructures from the NWs (at the lower NH_3 flow rate) to polyhedral crystal to nanobelts (at the higher NH_3 flow rate) in the thermal reaction of gallium oxide and NH_3 at 1100 °C. Juang and Chu [10] observed that decrease in the growth rate of GaN with increasing NH_3 flow rate. Lee et al. [11] revealed that the size and diameter of GaN nanostructure decrease with decreasing NH_3 flow rate. The advantages of NH_3 are as follows: (a) NH_3 is the most widely used source of nitrogen in the CVD process which dissociate at comparatively lower temperature than N_2, (b) NH_3 acts as a reducing agent which decreases the deposition rate, (c) NH_3 passivates the surface which further alters the ad-atom absorption, and (d) during the NW growth process, it acts as a ligand at metal-cap NWs [12]. The III/V ratio is an important parameter in a compound semiconductor to regulate its optical and electronic properties. It exhibits excellent surface passivation and minimal defect distribution in the GaN-NWs. Incorporation of nitrogen in the GaN-NWs network improves optoelectronic properties. Therefore, it is important to investigate the role of ammonia flow rate on chemical network and optical properties of GaN-NWs.

In this article, we investigate the effect of NH_3 flow rate on GaN-NWs and its phonon modes and we further correlate the vibrational properties with optical properties of GaN-NWs synthesized with different NH_3 flow rate.

✉ Bibhu P. Swain
bibhuprasad.swain@gmail.com; bibhu.s@smit.smu.edu.in

[1] Nano-Processing Laboratory, Centre for Material Science and Nanotechnology, Sikkim Manipal Institute of Technology, Majitar, Rangpo, East Sikkim 737136, India

[2] School of Advanced Material Engineering, Kookmin University, Seoul, Republic of Korea

2 Experimental details

Commercially available p-type Si (100) (resistivity: 1–3 Ω-cm) substrate was used in our experiment. The Si substrate was dipped in diluted hydrofluoric acid (2 % HF) solution for 2 min to remove the native oxide layer and then cleaned ultrasonically in deionized water for 15 min and then dried by nitrogen blowing. An 8-nm nickel thin film was deposited by sputtering technique followed by annealing at 700 °C in H_2 ambient environment for 1 h to form separate Ni nanoparticles (NPs). Then, the source and substrate were placed inside the reactor and pumped to subatmospheric pressure. We used gallium oxide (Ga_2O_3) to grow GaN-NWs in the presence of NH_3, H_2, and N_2 gases. Prior to the deposition, N_2 (99.99 %) gas was flowing to the reactor for 2 h in order to remove the residual gases. The furnace was heated to the growth temperature (1000 °C) at a rate of 5 °C/min. N_2 and H_2 flow rate was fixed at 200 and 50 sccm, respectively, while the NH_3 flow rate varied from 2 to 12 sccm. The deposition time was fixed for 4 h. After deposition, the furnace was cooled down gradually at a rate of 3 °C/min. The morphology of GaN-NWs was observed by atomic force microscopy (AFM). AFM study was done using Nanoscope III scanning probe microscope with a micro-fabricated Si_3N_4 cantilever (force constant 0.5 N m^{-1}) stylus assembly. The chemical network of GaN-NWs was studied by Fourier transform infrared spectroscopy (FTIR) and Raman spectroscopy. FTIR spectra were collected with a PerkinElmer spectrometer (Model: Spectrum 2) operating in transmission mode in the range 450–1000 cm^{-1} with a resolution of 1 cm^{-1}. The Raman spectrum was recorded with a Raman spectrometer (Horiba Jobin Yvon) at room temperature using the 488 nm line of an Ar^+ laser as an excitation source. The laser power on the spot of the GaN-NWs sample was ~1 mW to avoid any structural changes during analysis. Photoluminescence (PL) studies were conducted with a PerkinElmer LS-45 fluorescence spectrometer with a Xe discharge lamp operating at room temperature.

3 Result and discussion

3.1 Microstructure

Figure 1a, b shows the AFM image of GaN-NWs deposited at 6 and 12 sccm NH_3 flow rate in non-contact mode. The diameter of nanowires varies from 60 to 100 nm. Most of NWs are distributed in a random manner on the silicon substrate. Srivastava et al. [13] have deposited vertical GaN-NWs by vapor phase deposition on sapphire substrates and their NWs diameter of 40 nm and length extended up to 2 μm. Shaoo et al. [14] have observed short stature vertical GaN-NRs with diameter 100 nm deposited by thermal CVD. Johnson et al. [7] observed bunch of dense hairy GaN nanowires on Si substrate with diameter 20–500 nm and a length of 1–30 μm.

3.2 Bonding network

3.2.1 FTIR

Figure 2a shows the FTIR spectra of GaN-NWs in the range of 450–1000 cm^{-1}. The major vibration bands are observed in between 450 and 700 cm^{-1}. The vibration signatures of GaN-NWs exhibit six prominent peaks centered at 484, 532, 581, 637, 661, and 838 cm^{-1}. The vibration signature at 484, 532, 581, 637, 661, and 838 cm^{-1} is assigned to the zone boundary (ZB) phonon, A_1 (TO) phonon, E_2 (high), surface optic (SO) A, surface optic (SO) E, and defect-induced phonon, respectively. The significant observations are summarized as follows:

(a) The intensity of SO (A & E) and E_2 (high) increases with increasing NH_3 flow rate.
(b) The ZB phonon and the defect-induced phonon have very small change with NH_3 flow rate.
(c) The SO (E) phonon shows asymmetric nature toward higher wavenumber while A_1(TO) shows asymmetric nature toward the lower wavenumber with increasing NH_3 flow rate.
(d) The E_2 (high) and SO (A) phonon are more distinguishable with increasing NH_3 flow rate.

Enhancement of A_1 (TO) indicates the change of optical behavior in the GaN-NWs. The intensity of E_2 (high) phonon increases with increasing NH_3 flow rate. E_2 (high) phonon is usually used to analyze the stress in films. Therefore, it is confirmed that the higher NH_3 flow rate increases stress in the GaN-NWs network. The asymmetric nature of SO phonon could be due to different degree of surface roughness with different NH_3 flow rates.

Different vibrational signatures are overlapped in Fig. 2a. Therefore, we deconvoluted the FTIR spectra into eight individual Gaussian peaks. Figure 2b shows the deconvolution of the absorption vibration band from the 465 to 780 cm^{-1} of GaN-NWs synthesized at 12 sccm NH_3 flow rate. The peak appeared at 489.02, 510.20, 537.17, 587.78, 630.83, 659.65, 685.31, and 755.25 cm^{-1} are assigned as zone boundary (ZB) phonon, A_1 (TO), E_1 (TO), E_2 (high), SO (A), defect-induced (DI) phonon, SO (E), and E_1 (LO) phonon, respectively.

Figure 2c shows the variation in the peak position of various vibration signatures with increasing NH_3 flow rates. The peak position of ZB phonon shifts toward higher wave number from 487.7 to 490.53 cm^{-1} with an increasing NH_3 flow rate. These changes in the peak

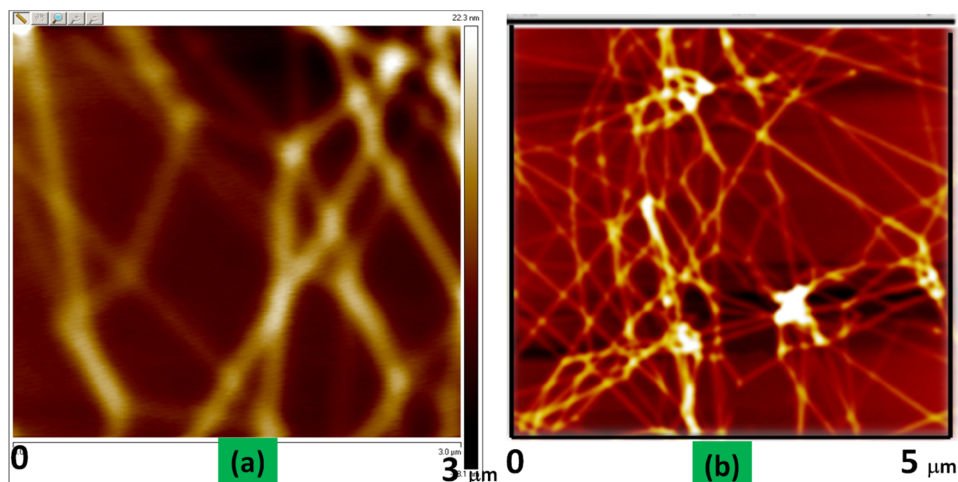

Fig. 1 AFM images of GaN-NWs synthesized with different NH_3 flow rate. **a** 6 sccm and **b** 12 sccm

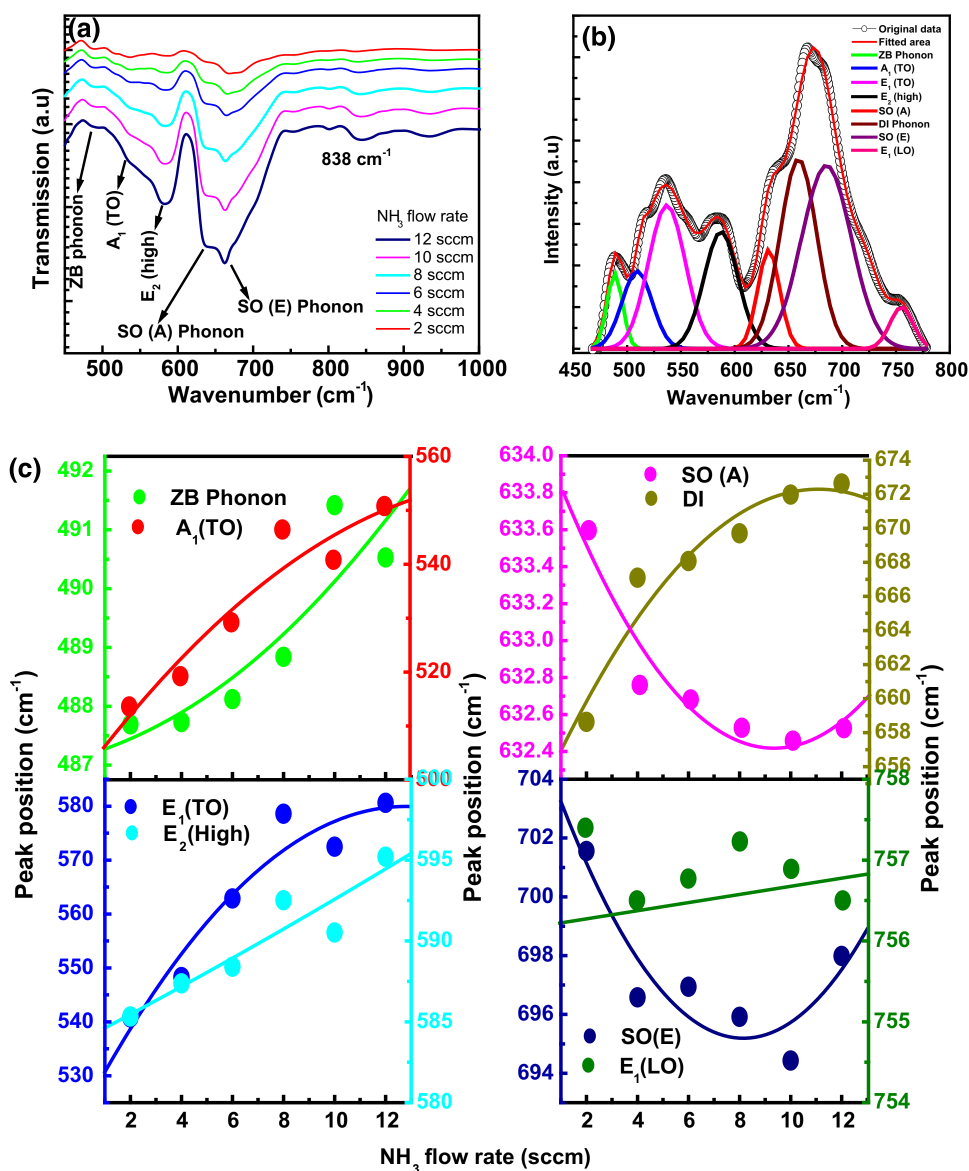

Fig. 2 **a** FTIR spectra of GaN-NWs synthesized with different NH_3 flow rate, **b** the deconvolution of FTIR spectra from 470 to 770 cm^{-1} into eight gaussian peaks, and **c** the variation of peak position of ZB phonon, A_1 (TO), SO (A), E_1 (TO), defect induced (DI), E_2 (High), SO (E), E_1 (LO) phonon mode of GaN-NWs at different NH_3 flow rate

position of the vibrational band cannot be attributed to a chemical change in NWs, but attributed to an atomic rearrangement in the NWs. On the other hand, the peak position of A_1 (TO) and E_1 (TO) phonon shifts from 513.63 to 550.8 and 540.83 to 580.6 cm^{-1}, respectively, with increasing NH_3 flow rate. Several factors may associated with shifting of TO toward higher wavenumber: (a) irregularity of NWs diameter, (b) stress in NWs, and (c) rearrangement of point defects due to nitrogen incorporation in the GaN network. The peak position of E_2(high) increases from 585.33 to 595.21 cm^{-1} with increasing NH_3 flow rates. In a similar manner, the peak position of SO (A) and SO (E) phonon shifted from 633.85 cm^{-1} to 632.56 and 697.99 to 701.56 cm^{-1}, respectively. A number of factors may lead to this effect (a) constrain of structural shape, (b) change of dielectric constant due to nitrogen incorporation, (c) surface roughness varies with different NH_3 flow rates, (d) defect distribution and nature of defects present in the nanostructure, and (e) surface modification or passivation of GaN-NWs. The E_1 (LO) phonon shifts from 756.5 to 757.4 cm^{-1}. Such a shift in LO phonon peak position indicates the existence of a multiphase system [15]. At 2 sccm NH_3 flow rate, the defect-induced (DI) phonon appears at 658.2 cm^{-1}; however, it appeared at 669.8 cm^{-1} when the NH_3 flow rate increased to 12 sccm.

3.2.2 Raman

Figure 3a shows Raman spectra in the range of 100 to 1300 cm^{-1} of GaN-NWs synthesized at different NH_3 flow rate. The various Raman active phonon modes were appeared at 234, 407, 515, 551, 590, 673, 792, 1120, and 1229 cm^{-1} corresponds to ZB phonon, acoustic overtone, A_1(TO), E_1 (TO), E_2 (high), SO (E) phonon, E_1 (LO), $2E_1$ (TO), $2E_2$ (high), respectively.

Some important observation in Raman spectra of GaN-NWs is as follows:

(a) The peak intensity of A_1 (TO) and E_1 (TO) phonon increases with increasing NH_3 flow rate.
(b) The small shoulder of E_2 (high) phonon decreases with increasing NH_3 flow rate.
(c) The peak intensity of SO phonon almost unchanged with increasing NH_3 flow rate.
(d) The full width at half maximum (FWHM) of LO phonon decreases, whereas its peak intensity sharply increases with increasing NH_3 flow rate.
(e) LO phonon also shows asymmetry toward higher wavenumber.

These abrupt changes in the phonon behavior of GaN-NWs may arise (a) due to mass defect and volume changes induced by incorporating nitrogen atom, (b) chemical shielding effect exerted by newly incorporated NH_3 moiety, and (c) change in internal stress of film due to the backing provided by rich electronegative nitrogen environments.

It is believed that the major part of NH_3 dissociates into negatively charged NH_2 and H^+ ion. The reactive H^+ ion has very high electron affinity, so that can easily attach to the GaN chemical network. On the other hand, the negatively charged NH_2^- ion is slower and often surrounded by bulky electron cloud. Therefore, it mainly occupied on the surface of NWs favoring nitrogen-rich environment of GaN.

Different vibrations are overlapped each other in the Raman spectra of GaN-NWs. Therefore, we have deconvoluted TO and LO phonon peak in the range of 460.70–647.70 and 730.08–833.63 cm^{-1} for GaN-NWs synthesized with 12 sccm NH_3 flow rate. Figure 3b shows the Gaussian fit of the A_1 (TO), E_1 (TO), and E_2 (high) phonons peak centered at 512.64, 543.91, and 582.30 cm^{-1}, respectively. Figure 3c shows A_1 (LO) and E_1(LO) phonons of GaN-NWs, centered at 762.49 cm^{-1} and 793.32 cm^{-1}, respectively. Figure 3d shows the shift in peak positions and FWHM of A_1 (TO), E_1 (TO), E_2-(high) phonon mode of the GaN-NW. These results are in accordance with Fig. 3b. The peak position of A_1 (TO) phonon shifts from its 513.54 cm^{-1} 517.79 cm^{-1} with increasing NH_3 flow rate and their respective FWHM also increases from 36.459 to 42.619 cm^{-1}, respectively. The shifting of A_1 (TO) phonon to the higher frequency region could be due to steric or crowding effect caused by continuous incorporation of nitrogen or hydrogen moiety in GaN network, whereas increasing of its FWHM is due to increase in disorder. From these experimental results, it is acceptable to us that the increasing of NH_3 flow rate adversely affects the overall properties of GaN-NWs. In a similar trend, the peak position and FWHM of E_1 (TO) phonon shifted from 545.7 to 556.88 and 49.385 to 55.928 cm^{-1} with increasing NH_3 flow rate. Generally, Raman peak position shows shift, widen and asymmetric with the size of nanomaterials. The peak position of E_2 (high) phonon shifts from 576.54 to 597.08 cm^{-1}, whereas FWHM of E_2 (high) increases from 33.45 to 40.66 cm^{-1} with increasing NH_3 flow rate. The shifting of peak position to higher frequency and increasing FWHM could be attributed to increase in stress in the film due to continuous nitrogen incorporation [16]. Figure 3e shows peak positions and FWHM of A_1(LO) and E_1 (LO) phonon of GaN-NWs deposited with different NH_3 flow rate. The peak position of A_1 (LO) shifts toward higher wave number region, which varies from 762.69 to 763.87 cm^{-1} with an increasing of NH_3 flow rate and their respective FWHM decreases from 25.571 to 19.928 cm^{-1}. The shift of peak

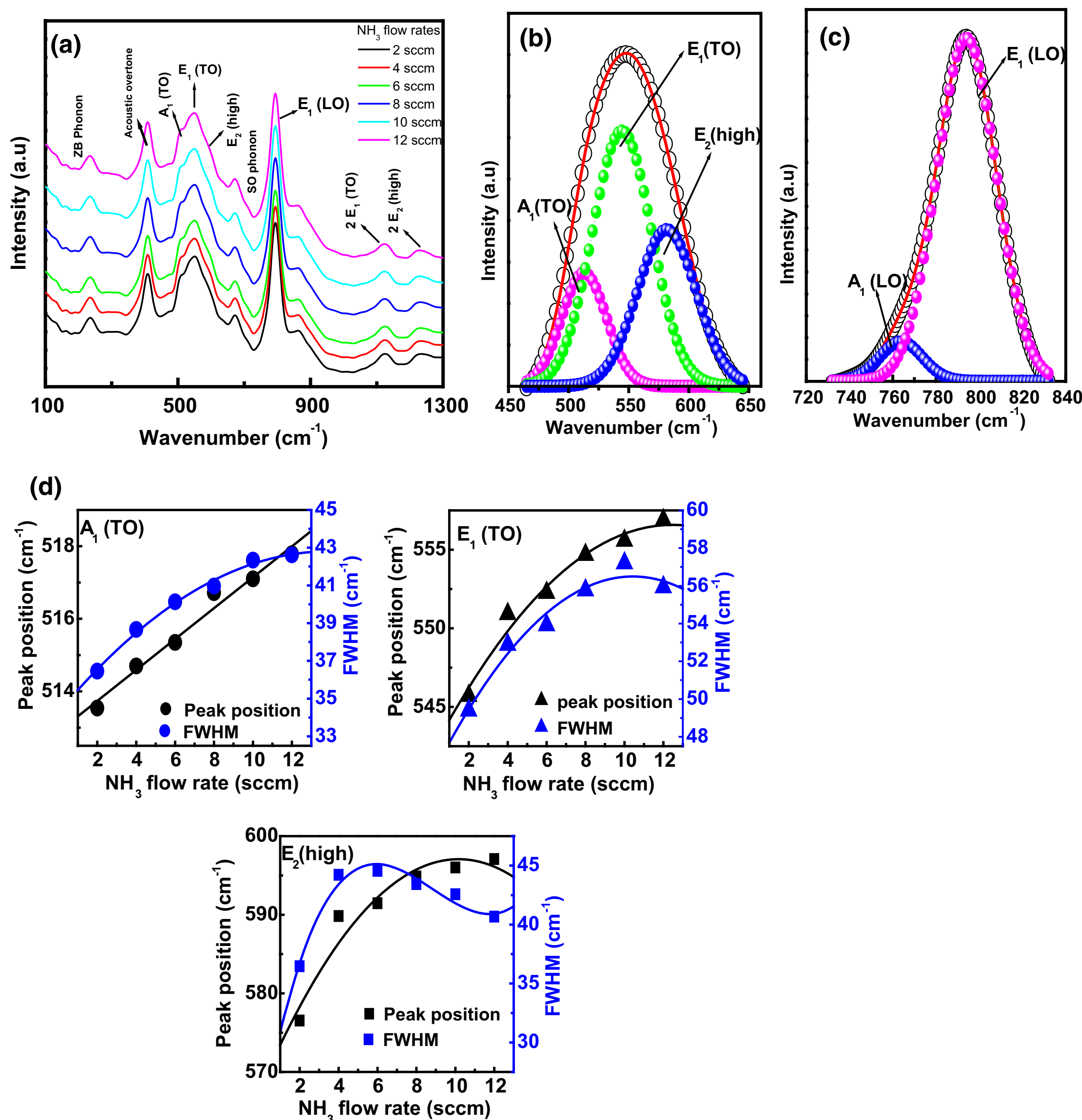

Fig. 3 **a** Raman spectra of GaN-NWs deposited with different NH_3 flow rate, **b** deconvolution of Raman spectra from 450 to 650 cm^{-1} into A_1 (TO), E_1 (TO), and E_2 (high) at 12 sccm NH_3 flow rate, **c** deconvolution of Raman spectra from 720 to 830 cm^{-1} into A_1 (LO) and E_1 (LO) at 12 sccm NH_3 flow rate, **d** the variation of peak positions and FWHM of A_1 (TO), E_1 (TO), E_2 (high) phonon at different NH_3 flow rate, **e** the variation of peak position and FWHM of A_1 (LO) and E_1 (LO) phonon at different NH_3 flow rate, **f** the ratio of $I_{E1(LO)}$ and $I_{A1(LO)}$ ($I_{E1(LO)}/I_{A1(LO)}$) and the ratio of $FWHM_{E1(LO)}$ and $FWHM_{A1(LO)}$ ($FWHM_{E1(LO)}/FWHM_{A1(LO)}$), **g** the ratio of $I_{E1(TO)}$ and $I_{A1(TO)}$ ($I_{E1(TO)}/I_{A1(TO)}$) and the ratio of $FWHM_{E1(TO)}$ and $FWHM_{A1(TO)}$ ($FWHM_{E1(TO)}/FWHM_{A1(TO)}$), and **h** $\omega_{E1(LO)} - \omega_{A1(LO)}$ and $\omega_{E1(TO)} - \omega_{A1(TO)}$ phonon of GaN-NW deposited with different NH_3 flow rate

position to higher wavenumber is due to the presence of stress in the film, whereas a decrease in FWHM indicates increase in crystallinity. This further indicates that higher flow rates of NH_3 gas are required to yield sufficient amounts of active nitrogen species (N, NH, NH_2) for GaN-NWs growth. However, an increasing of NH_3 flow rate may increase stress in the film and intensify impurity diffusion. On the other hand, the peak position and FWHM of E_1 (LO) peak decreases from 794.34 to 794.11 and 28.211 to 27.619 cm^{-1} with increasing NH_3 flow rates, respectively. The peak shift toward lower wavenumber is due to size effect, whereas a decrease in FWHM indicates the improved crystallinity of GaN-NWs film. Though NH_3 is the most commonly used nitrogen sources for GaN deposition, it has also the disadvantage of being extremely corrosive.

We plotted the ratio of the integrated intensity of E_1(LO) to A_1(LO), ($I_{E1(LO)}/I_{A1(LO)}$) and their ratio of

Fig. 3 continued

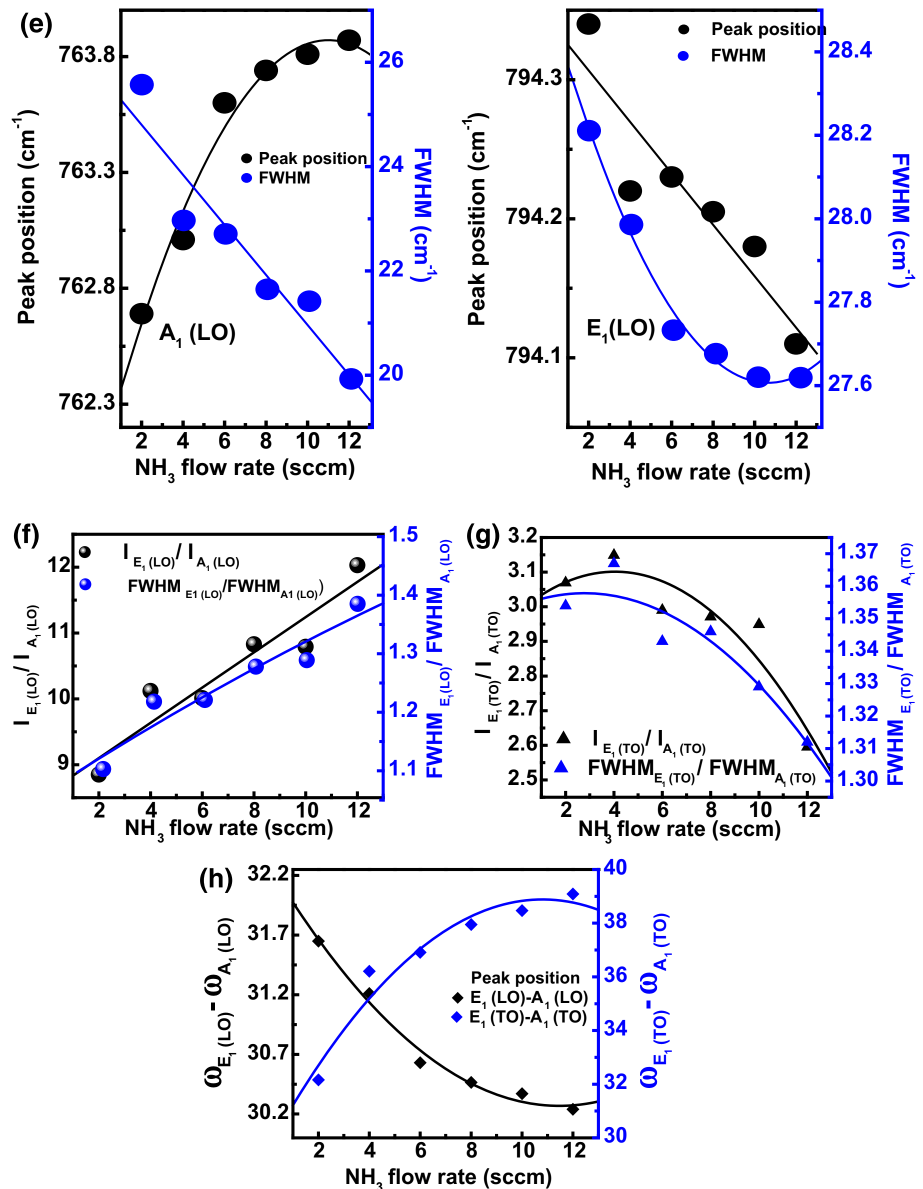

respective FWHM ($FWHM_{E1(LO)}/FWHM_{A1(LO)}$) (Fig. 3f) and the ratio of integrated intensity E_1(TO) to A_1(TO), ($I_{E1(TO)}/I_{A1(TO)}$) and their ratio of respective FWHM ($FWHM_{E1(TO)}/FWHM_{A1(TO)}$) (Fig. 3g). Figure 3h shows the difference in the peak position of E_1(LO) and peak position of A_1(LO), ($\omega E_1(LO) - \omega A_1(LO)$); and the difference in the peak position of E_1(TO) and peak position of A_1(TO), ($\omega E_1(TO) - \omega A_1(TO)$) of GaN-NW deposited with different NH_3 flow rates. As the A_1 and E_1 symmetry belongs to polar phonons, the chemical network analysis may reveal the polarity behavior of GaN-NWs. An obvious reason of the stress relaxation is the atomic intermixing at the Si–GaN interface. The degree of the interface intermixing can be determined by the integrated peak intensity ratio of two phonons as the intensity depends on the relative number of corresponding bonds. The integrated intensity ratio may depend strongly on the crystal orientation and surface property of material. $I_{E1(LO)}/I_{A1(LO)}$ which increases from 10.12 to 12.03 and their respective $FWHM_{E1(LO)}/FWHM_{A1(LO)}$ also increases from 1.218 to 1.385 with increasing NH_3 flow rate. This indicates an increase in crystalline quality of GaN-NWs with increasing NH_3 flow rate. On the other hand, $I_{E1(TO)}/I_{A1(TO)}$ decreases from 3.069 to 2.595 and their respective $FWHM_{E1(TO)}/FWHM_{A1(TO)}$ also decreases from 1.354 to 1.312. Here, we can consider that the decrease in the ratio of FWHM and ratio of the integrated peak intensity arises due to directional asymmetric; as a result, phonon movement is constrained. Similarly, the difference in the peak position of E_1(LO) and A_1(LO) decreases from 31.65 to 30.24,

whereas the difference in the peak position of E_1(TO) and A_1(TO) peak increases from 32.16 to 39.09. This anomalous behavior of phonon could be correlated with unequal bond polarity imposed by unequal distribution of N molecules around GaN chemical environment.

3.3 PL analysis

Figure 4a shows the room temperature PL spectra of GaN-NWs deposited with different NH_3 flow rates. The excitation wavelength was fixed at 330 nm (3.75 eV). The excitation energy is higher than the band gap of bulk GaN (3.4 eV). Therefore, in this particular PL analysis, we have examined the surface states of GaN-NWs. The broad PL spectrum spreads from 388 to 513 nm. Two distinct emission peaks were observed at 2.81 and 2.95 eV which lies at the lower energy region as compared to its bulk counterpart (3.4 eV). Such a lowering of band gap energy of GaN-NWs was previously reported in the literature and it is assigned to the presence of nitrogen vacancy in the NWs [17]. The appearance of PL peak at 2.81 eV corresponds to blue emission from GaN [18]. The FWHM of PL peaks increases from 0.37 to 0.39 eV with increasing NH_3 flow rate from 4 to 10 sccm. However, an irregularity was observed in case of 12 sccm NH_3 flow rate. This increase in FWHM may be due to the increasing number of defects with higher NH_3 flow rate. Some important observations are addressed as follows:

(a) The broad emission band spreads over 2.4–3.19 eV. These could be due to the incorporation of nitrogen in GaN network.
(b) The prominent blue emission from GaN-NWs was observed at 2.81 eV. The blue emission may be due to crystal defects such as V_{Ga}-complexes. The dangling bonds at Ga atoms mostly contribute to the deep-gap states, whereas those of introducing N atoms in the GaN-NWs contribute to the valence-band tails.
(c) The PL intensity that increases with increasing NH_3 flow rates could be due to quantum confinement effect. Defects and impurities provide new states for electrons and holes, altering their motion, lifetime, and transition energies.

Purushothaman et al studied the PL spectra of GaN-NWs synthesized at a NH_3 flow rate of 500 and 200 sccm [19]. They observed strong UV-near band edge emission at 3.4 eV and relatively weak emission band at the lower energy side (2.2–3.1 eV) appears due to structural defects [19]. Shekari et al. [4] revealed that the broadening of PL peak is due to the lesser quantum confinement effect of the

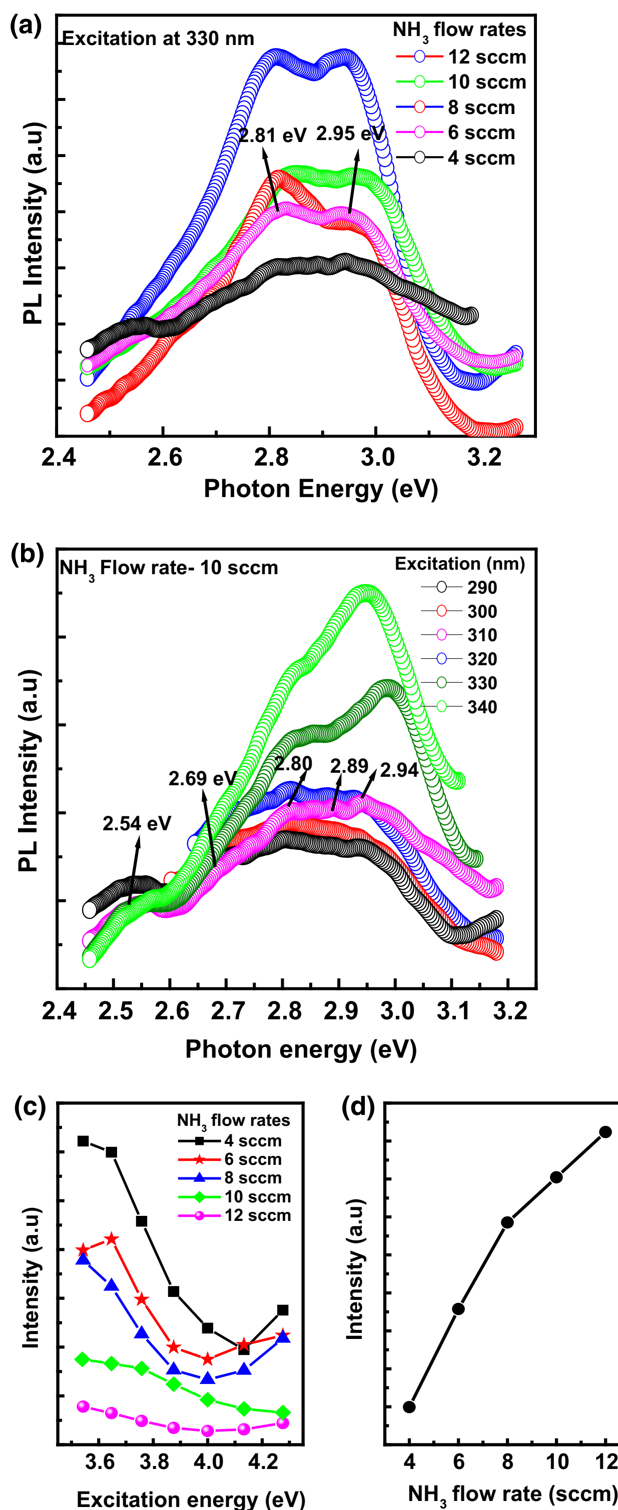

Fig. 4 **a** PL spectra of GaN-NWs deposited with different NH_3 flow rate excited at 330 nm, **b** PL spectra of GaN-NWs deposited at 10 sccm NH_3 flow rate with varied excitation energy from 290 to 340 nm, **c** the integrated PL intensity of GaN-NWs with different excitation energy from 3.54 to 4.45 eV, and **d** variation of the integrated intensity with different NH_3 flow rate

as-grown crystalline structure, whereas shifting in PL peak is related to the quality of the NWs and it is determined by the number of luminescent centers and relaxation of thermally charged carriers. Figure 4b shows the PL spectra of GaN-NWs excited by different excitation wavelength. It shows a broad range emission band between 2.4 and 3.2 eV with a maximum peak centered at 2.95 eV (blue emission). However, it is seen that GaN-NWs sample synthesized at 10 sccm NH_3 flow rate shows five emission band centered at 2.54 (488 nm), 2.69 (461 nm), 2.80 (442 nm), 2.89 (429 nm), 2.94 (421 nm) eV, respectively. These emission peaks are probably associated with the deep or defect levels [20]. The slight red shift can be attributed to the strain in GaN-NWs. The intensity of the emission band became stronger with increase in excitation wavelength. Defects and impurities break the lattice periodicity and perturbed the band structure locally in the GaN-NWs. The surfaces and interfaces of nanowires usually contain a high concentration of impurity and defect states. In particular, the dangling bonds on the GaN-NWs often provided numerous midgap states that facilitate rapid nonradiative recombination. Because the surface recombination is usually nonradiative, band bending can lead to the formation of a depletion region or dead layer where PL is effectively quenched, both of these phenomena lead to reduce the PL intensity of GaN-NWs. Figure 4c shows the integrated PL intensity of GaN-NWs samples with different excitation energy. From this figure, it is observed that the integrated PL intensity decreases with increase in excitation energy. A decrease in the integrated PL intensity implies non-uniform distribution of surface states. Figure 4d shows the plot of the integrated PL intensity of GaN-NWs samples with different NH_3 flow rates. It is evident that the integrated PL intensity increases with increasing NH_3 flow rates. This increase in PL intensity is related to the extra hydrogen available during the growth process. It is believed that this extra hydrogen atom will effectively passivate the defect center at the surface of NWs.

4 Conclusion

GaN-NWs were synthesized using Ni catalyst with varying NH_3 flow rate. We observed that the NH_3 flow rate not only affects the morphology, but also modifies chemical network and optical properties of GaN-NWs. Enhancement of A_1 (TO) phonon with increasing NH_3 flow rate indicates the change of optical behavior in the GaN-NWs. The PL intensity increased with increasing of NH_3 flow rate due to the passivation/modification of the GaN-NWs surface.

Acknowledgments This study was partly supported by the Department of Science and Technology, Govt. of India (Project No: SB/FTP/ETA-295/2011). Umesh Rizal acknowledged the financial support from JRF scheme under the Department of Biotechnology, Government of India (Project No: BCIL/NER-BPMC/2012/650).

References

1. C.P. Chen, A. Ganguly, C.Y. Lu, T.Y. Chen, C.C. Kuo, R.S. Chen, W.H. Tu, W.B. Fisher, K.H. Chen, L.C. Chen, Anal. Chem. **83**, 1938–1943 (2011)
2. J. Goldberger, R.R. He, Y. Zhang, S. Lee, H. Yan, H.J. Choi, P. Yang, Nature **422**, 599–602 (2003)
3. E.A. Stach, P.J. Pauzauskie, T. Kuykendall, J. Goldberger, R.R. He, P. Yang, Nano Lett. **3**, 867–869 (2003)
4. L. Shekari, A. Ramizy, K. Omar, H.A. Hassan, Z. Hassan, Appl. Surf. Sci. **263**, 50–53 (2012)
5. J. Chen, C. Xue, H. Zhuang, H. Li, L. Qin, Z. Yang, J. Mater. Process. Technol. **208**, 255–258 (2008)
6. C.Y. Nam, D. Tham, J.E. Fischer, Appl. Phys. Lett. **85**, 5676–5678 (2004)
7. J.L. Johnson, Y. Choi, A. Ural, J. Vac. Sci. Technol. B. **26**, 1841–1847 (2008)
8. Y. Lan, F. Lin, Y. Li, Z. Yang, H. Zhou, Y. Lu, J. Bao, Z. Ren, M.A. Crimp, J. Cryst. Growth **415**, 139–146 (2015)
9. S. Sundaram, S. Lourdudoss, G. Landgren, K. Baskar, J. Cryst. Growth **312**, 3151–3155 (2010)
10. F.S. Juang, T.H. Chu, J. Cryst. Growth **225**, 145–149 (2001)
11. S.S. Lee, C.S. Kim, N.M. Hwang, Aerosol. Sci. Tech. **46**, 1100–1108 (2012)
12. X. Wen, W. Zhang, S. Yang, Nano Lett. **2**, 1397–1401 (2002)
13. V. Srivastava, V. Sureshkumar, D. Puvia, K. Thangaraju, R. Thangavel, J. Kumar, J. Cryst. Growth **275**, E2367–E2369 (2005)
14. P. Shaoo, S. Dhara, S. Dash, A.K. Tyagi, Nanosci Nanotechnol Asia **1**, 140–170 (2011)
15. M.F. Cerqueira, M.I. Vasilevskiy, F. Oliveira, A.G. Rolo, T. Viseu, J. Ayres, D. Campos, E. Alves, R. Correia, J. Phys. Condens. Mater. **23**, 1–6 (2011)
16. R.P. Parikh, R.A. Adomaitis, J. Cryst. Growth **286**, 259–278 (2006)
17. X. Xiang, C. Cao, Y. Xu, H. Zhu, Nanotechnology **17**, 30–34 (2006)
18. M.A. Reshchikov, H. Morkov, J. Appl. Phys. **97**, 61301–613095 (2005)
19. V. Purushothaman, V. Ramakrishnan, K. Jeganathan, CrystEngComm **14**, 8390–8395 (2012)
20. A. Sedhain, J. Li, J.Y. Lin, H.X. Jiang, Appl. Phys. Lett. **96**, 1519021–1519023 (2010)